DESIGN OF BESPOKE MERRITT-BRAUNBECK COILS WITH IMPROVED OPTICAL ACCESS FOR QUANTUM SENSING

Ma Weiyi[1], Peng Yuan Han[2], Wee Wei Hsiung[2]
[1] Dunman High School, 10 Tanjong Rhu Road, Singapore 436895
[2] DSO National Laboratories, 12 Science Park Drive, Singapore 118225

Abstract

Magnetic coils are crucial to quantum-related experiments as homogenous magnetic fields provide quantization axes for sensing and enables precise control over quantum states. The design of magnetic coils needs to ensure uniformity and field strength, which is further complicated by geometric requirements for optical access. We conceptualize, build, and analyze bespoke magnetic coils inspired by the Merritt and Braunbeck configurations for the generation of strong and homogenous fields with improved optical access. This compact novel configuration provides a field that deviates by less than 1% across more than 70% of the coil length, providing strong magnetic fields over large spatial volumes with the potential to significantly reduce noise and optical restrictions in quantum systems.

1 Introduction

Magnetic fields play an indispensable role in many areas of scientific research, namely for various precision measurements. In the context of quantum mechanics, magnetic fields are required in a plethora of situations, such as the trapping and laser cooling of atoms [1], and to provide a quantization axis for sensing. Such applications serve as the fundamental basis of more complex set-ups, including magneto-optical traps for cold atom interferometry [2].

The generation of homogenous or gradient magnetic fields requires specific, stable, and well-controlled environments. Even the most miniscule deviations from these optimal magnetic field profiles, often due to the unwanted presence of stray signals, will greatly disturb quantum states and result in skewed findings. For instance, cold atom interferometry experiments investigating the universality of free fall using atoms are highly sensitive to infinitesimal changes in magnetic fields of the spatial trajectory through which the atoms travel through. If irregularities in magnetic fields cause the atoms' trajectory to fall off the intended axis of the sensor, the system will become susceptible to external interference [3]. These detriments are exacerbated when sensors using magnetic fields are operated in environments where large background fields change both spatially and temporally.

Various coil configuration geometries have been devised to create suitable magnetic fields, including the solenoid, Helmholtz [4], Braunbeck [5], and Merritt [6] coil geometries, which have had sustained success during utilization in many experiments and remain as popular choices for the generation of uniform magnetic fields. However, many currently-existing coil geometries are constrained by its range of optical access. While ubiquitous coil geometries may prove to be versatile in creating uniform or gradient magnetic fields, optical access acts as a major constraint when performing measurements [7]. It is best for a spacious view of the region of interest to be

available, but the presence of bulky coils and other opaque materials present within the experimental setup creates inaccessible areas that block the path of lasers, restricting the spatial range for which measurements and observations can be obtained.

We are hence motivated to create bespoke coil configurations with the primary goal to mitigate background magnetic fields and to improve the range of optical access within experimental set-ups. In this paper, we design and build a novel coil system that posits greater visibility for measurements, whilst numerically maximising the uniformity of the generated magnetic field. In Section 2, we compare the properties of existing coil geometries (Helmholtz, Braunbeck, and Merritt four-coil) and investigate the homogeneity of their fields through numerical means and computational simulations. Next in Section 3, we characterise and construct a bespoke coil system based on the findings in the previous section. We analyse our resultant model in Section 4, detailing the results obtained by our methodology. Lastly, in Section 5, we provide discussions and future directions regarding our findings, thereby concluding the paper.

2 Preliminary Analysis

To provide insights for the design of our coil system, we first investigate currently-existing coil geometries, namely the Helmholtz, Braunbeck, and Merritt four-coil systems, through the characterisation of their magnetic flux density, as well as the overall homogeneity of their respective fields. To calculate the magnetic field **B** generated by each coil system, we use the fundamental equation of the Biot-Savart law as shown below

$$\boldsymbol{B} = \frac{\mu_0}{4\pi}\int_C \frac{Id\ell \times \boldsymbol{r}'}{|\boldsymbol{r}'|^3}$$

where μ_0 is the permeability of free space, $d\ell$ is an infinitesimal segment of a path C, I is the current through the path, and $\boldsymbol{r}' = \boldsymbol{r} - \ell$ is the displacement vector from $d\ell$ at a point ℓ along C, to the point $\boldsymbol{r}$ at which the field is being computed. Consider a circular coil of radius R (m) carrying a current I (A) with n turns of the wire. For a point of a distance x (m) away along the centre axis of the aforementioned loop, the magnetic flux density B in the axial direction is given as follows.

$$B = \frac{\mu_0 nIR^2}{2(R^2 + x^2)^{\frac{3}{2}}}$$

Consider a similar square coil with side length L (m). The magnetic flux density at a point of distance x away is shown.

$$B = \frac{\mu_0 nIL^2}{2\pi}\left[\frac{1}{\left(x^2 + \frac{1}{4}L^2\right)\sqrt{x^2 + \frac{1}{2}L^2}}\right]$$

In a Helmholtz coil configuration, two identical circular coils with radius R are placed symmetrically along a common axis, carrying electrical currents of equal magnitude and direction, as shown in Fig. 1. The key characteristic of a Helmholtz configuration is that the separation of

both coils is equal to the radius of both coils, thereby providing a uniform field. Using the Biot-Savart law and the superposition principle, the overall magnetic flux density at the origin can be found by adding the magnetic fields generated by each individual coil, as shown.

$$B_z = 2 \times \frac{\mu_0 n I R^2}{2\left[R^2 + (\frac{1}{2}R)^2\right]^{\frac{3}{2}}} = \frac{8\sqrt{5}}{25} \times \frac{\mu_0 n I}{R} = \frac{0.7155 \mu_0 n I}{R}$$

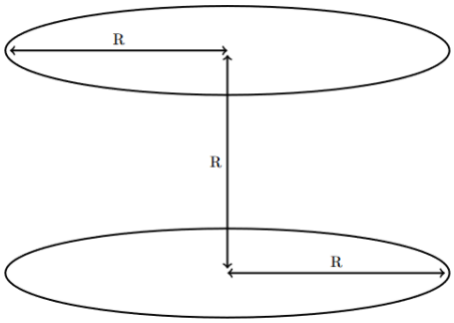

Figure 1. *A Helmholtz coil configuration.*

The Braunbeck coil configuration is a modified version of the Helmholtz configuration, as shown in Fig. 2. Two pairs of coils are placed symmetrically along a common axis, each carrying a current of equal magnitude and direction. The radius and separation of each pair of coils is determined by various ratios to optimise the uniform field at the centre [8]. The corresponding ratios and the magnetic flux density generated by the Braunbeck configuration are shown below, where a_1 is the radius of the outer coils, a_2 is the radius of the inner coils, d_1 is the distance between the outer coil and the centre, and d_2 is the distance between the inner coil and the centre.

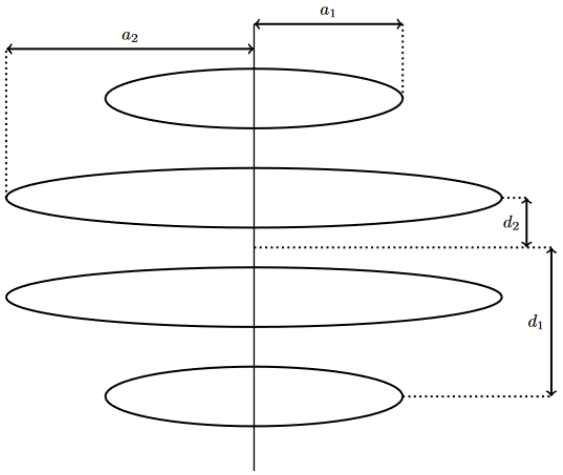

Figure 2. *A Braunbeck coil configuration.*

$$\frac{a_2}{a_1} = 1.30907, \qquad \frac{d_1}{a_1} = 1.10704, \qquad \frac{d_2}{a_1} = 0.36396, \qquad \frac{d_2}{a_2} = 0.27803$$

$$B_z = 2 \times \frac{\mu_0 n I a_1^2}{2(a_1^2 + d_1^2)^{\frac{3}{2}}} + 2 \times \frac{\mu_0 n I a_2^2}{2(a_2^2 + d_2^2)^{\frac{3}{2}}} = \frac{1.28860 \mu_0 n I}{a_2}$$

The Merritt four-coil system, illustrated in Fig. 3, uses square coils instead of circular coils as commonly seen before in Helmholtz and Braunbeck configurations. Two pairs of square coils, equal in length, are symmetrically placed along a common axis. The ratios of the distance a from the origin to the inner pair of coils, the distance b from the origin to the outer pair of coils, and the side length L are specified [9]. Furthermore, the ratio of the ampere-turns in the inner pair of coils $n'I'$ to that in the outer pair of coils nI is also shown.

$$\frac{a}{L} = 0.128106, \qquad \frac{b}{L} = 0.505492, \qquad \frac{n'I'}{nI} = 0.423514$$

For a Merritt four-coil system, the magnetic field is thus

$$B_z = 2\frac{\mu_0 L^2}{2\pi}\left[\frac{n'I'}{\left(a^2 + \frac{1}{4}L^2\right)\sqrt{a^2 + \frac{1}{2}L^2}} + \frac{nI}{\left(b^2 + \frac{1}{4}L^2\right)\sqrt{b^2 + \frac{1}{2}L^2}}\right] = \frac{0.71428 \mu_0 n I}{L/2}$$

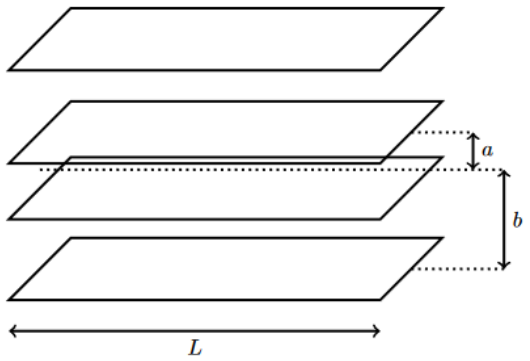

Figure 3. *A Merritt four-coil configuration.*

To analyse the homogeneity of the fields generated by each coil geometry, we employ metrics describing an "acceptably homogeneous" length as a proportion of the dimensions of the coils along each axis. We define a length to be "acceptably homogenous" if the magnetic flux density of all points along the length fall within 99% of the magnetic flux density experienced at the origin. For simplicity, when discussing square coils, we will refer to the side length as a "diameter", and one-half of the side length as a "radius". For the radial axis, we define the metric to be a percentage of d/D, where d is the length of the acceptably homogenous space along the radial axis and D is the diameter of the innermost coil. Similarly, along the axial, we define the metric to be z/H, where z is the length of the acceptably homogenous space along the axial axis and H is the separation between the two innermost coils.

Furthermore, it is theoretically optimal for each coil to be filamentary, that is, to be infinitely small and narrow, bearing negligible thickness. However, real coils must have some finite width and thickness due to the physical diameter of the wire and the number of turns. Different coiling methods will naturally result in variations to any measurements, hence it may be helpful to discuss some specific coiling methods, namely helical coiling and pancake coiling. Helical coiling involves loops of a constant diameter being coiled next to each other, like a solenoid. Pancake coiling involves loops coiled in an outward spiral, increasing the diameter of each successive loop. The analysis for field homogeneity will be performed for filamentary, helical, and pancake coils to account for the differences caused by each coiling method.

For precise simulations and computations of the magnetic flux density, we use Magpylib, an open-source Python library using vectorised field computation, to calculate the static magnetic fields generated by the current coil geometries [10]. Using Magpylib, we construct each of the three coil geometries articulated prior, setting the current to one ampere. The filamentary setup only has one turn of wire, whereas the helical and pancake coils each have 5 turns of wire within a space of 0.25 arbitrary units. We then create sensor paths to calculate the magnetic flux density along the radial and axial axes at regular intervals, after which we use NumPy and Matplotlib to calculate the metrics involving acceptably homogenous spaces. The results are shown in Table 1. Plots for these values are included in the Annex.

Coil geometry	Coiling method	d/D (%)	z/H (%)
Helmholtz	Filamentary	37.78	31.38
	Helical	37.98	31.25
	Pancake	42.16	28.69
Braunbeck	Filamentary	61.10	213.74
	Helical	61.34	213.19
	Pancake	64.46	195.34
Merritt four-coil	Filamentary	64.53	281.42
	Helical	64.74	280.79
	Pancake	67.74	258.38

Table 1. *Proportions of homogenous fields for each coil geometry.*

3 Model & Methodology

Our preliminary findings show that the Braunbeck coil configuration offers the strongest magnetic fields in terms of radius of half side-length, evident from its parametric equation derived from the Biot-Savart law. On the other hand, the Merritt four-coil configuration offers the greatest extent of an acceptably homogenous space, achieving the upper hand for all coiling methods when compared to both Helmholtz and Braunbeck configurations. Furthermore, the square design of the Merritt coils provides a larger boundary as compared to the traditional usage of circular coils, acting as a crucial aid in improving the optical access of experimental setups, thereby allowing for more accurate measurements to be taken from a wider variety of angles and perspectives. The respective strengths of the Braunbeck and Merritt coil configurations prompts us to investigate the properties of a combination between the two aforementioned designs, as their fusion may posit the ability to generate stronger magnetic fields with greater homogeneity, accompanied by a larger space for optical access that allows for a higher degree of freedom for observations to be obtained. We term this configuration a Merritt-Braunbeck configuration, and visualise this configuration to

be similar to that of a Braunbeck coil configuration, simply with square coils replacing the circular coils. This forms the basis of our bespoke magnetic coil design. Due to this modification, the optimal ratios for radii and separation may differ for a Merritt-Braunbeck configuration, hence requiring further investigation to be made regarding the best dimensions for the configuration.

In order to determine the best separation and dimensions for the Merritt-Braunbeck coil configuration, we adopt a numerical and computational approach to systematically estimate the optimal ratios, which is done using SciPy's optimiser algorithms. SciPy is a widely-used Python library for scientific computing, equipped with a diverse slew of mathematical functions and algorithms [11]. SciPy's optimiser algorithms focuses on minimisation, taking a parametric function alongside an array of initial guesses and employing mathematical algorithms to return an array of parameters that provide a minimised output. SciPy boasts many different optimisation methods, ranging from Newton's conjugate-gradient method to Powell's method. For the purposes of our research, we utilise the Nelder-Mead simplex algorithm for the minimisation of our multivariate field homogeneity function [12]. Setting a_1 equal to 1 arbitrary unit, we pass in a parameter tuple of 3 elements representing a_2, d_1, and d_2, following the original ratios for a regular Braunbeck configuration, which acts as reasonable initial guesses. Within the field homogeneity function, a magnetic field is simulated using the parameter tuple for the dimensions and separation of a filamentary Merritt-Braunbeck configuration. For the majority of dimensions chosen, the acceptably homogenous space along the axial axis was enough to last beyond the two innermost coils, thereby practically eliminating the need to optimise using the z/H metric. Hence, the d/D metric was used as a singular objective function with its reciprocal minimised using the three dimensions within the parameter tuple. After several rounds of tuning, the ratios obtained by the minimisation optimiser are as shown, providing a radial homogenous length of approximately 86.07% and an axial homogenous length of approximately 127.02%.

$$\frac{a_2}{a_1} = 1.40, \qquad \frac{d_1}{a_1} = 0.67889, \qquad \frac{d_2}{a_1} = 0.19856$$

With the ratios obtained, we now construct the physical setup. The setup is prepared with the flatter side of the frames facing towards the ground, and built in a vertical manner. Following the ratios given above, we let a_1 = 50mm, a_2 = 70mm, d_1 = 33.94mm, and d_2 = 9.93mm. Each frame is 7mm tall and 7mm thick, with a 5mm width in the middle indented by 5mm inwards to hold the wires. Prongs are designed to protrude from each of the 4 corners of the frames, with holes of a diameter of 5.5mm. This is such that rods can be slotted through the holes, along with stoppers, to provide structural and mechanical support for the entire setup. The 3-dimensional models for the smaller frame and the larger frame are shown in Fig. 4a and Fig. 4b respectively. The frames, rods, and stoppers are 3D-printed using PLA+ filaments. Each frame is helically coiled in the same direction with 4 turns of enamelled copper wire measuring 1.12mm in diameter (CUL 1,12, BLOCK Transformatoren-Elektronik GmbH). The metal wires between each frame are connected using clips to provide a closed circuit, and the remaining ends are connected with a D.C. power supply, providing an electrical amperage of 1A to the entire setup. The completed setup is depicted in Fig. 4c.

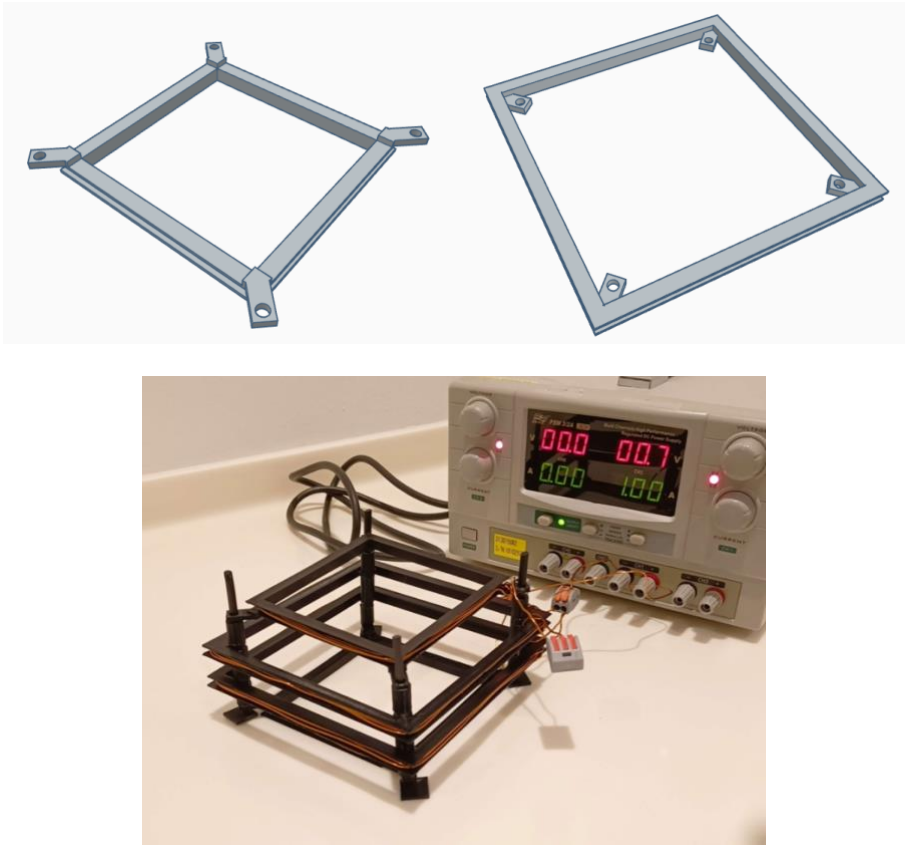

Figure 4. *3D models of the* ***(a)*** *smaller, outer frame and the* ***(b)*** *larger, inner frame, alongside* ***(c)*** *the real-life coiled frames complete with rods and stoppers.*

For the physical sensing of the magnetic field, we employ a triple-axis D.C. gaussmeter (VGM model, AlphaLab Inc.), equipped with a measurement range of $\pm 799.99 Gs$ and a relative error of measurement of $\pm 1\%$ in room temperatures. The probe of the gaussmeter contains the physical sensors oriented in the x, y, and z axes, with the dimensions of the probe measuring 6.3mm by 6.3mm by 50mm. The magnetometer is inserted into the setup along the radial and axial axes, and measurements of the magnetic flux density across all axes, as well as the overall magnitude of the field, are taken at regular intervals of 5mm.

4 Results

Mathematically, the parametric equation describing the magnetic flux density generated by the filamentary Merritt-Braunbeck coil configuration is as shown, using the optimised ratios found in Section 3.

$$B_z = 2\frac{\mu_0 nI}{2\pi}\left[\frac{(2a_1)^2}{\left(d_1^2+\frac{1}{4}(2a_1)^2\right)\sqrt{d_1^2+\frac{1}{2}(2a_1)^2}}+\frac{(2a_2)^2}{\left(d_2^2+\frac{1}{4}(2a_2)^2\right)\sqrt{d_2^2+\frac{1}{2}(2a_2)^2}}\right]$$
$$= \frac{1.65597\mu_0 nI}{a_2}$$

Now, we describe our computational and simulated results. As mentioned in the prior section, Magpylib simulations show that the optimised ratios provide a radial homogenous length of 86.07% and an axial homogenous length of 127.02%. The magnetic flux density across the radial and axial axes are depicted in Fig. 6a and Fig. 6b. The green line represents the upper bound for the homogeneity threshold, and the orange line represents the lower bound for the homogeneity threshold. The red points represent the points at which the magnetic field first stops being acceptably homogenous.

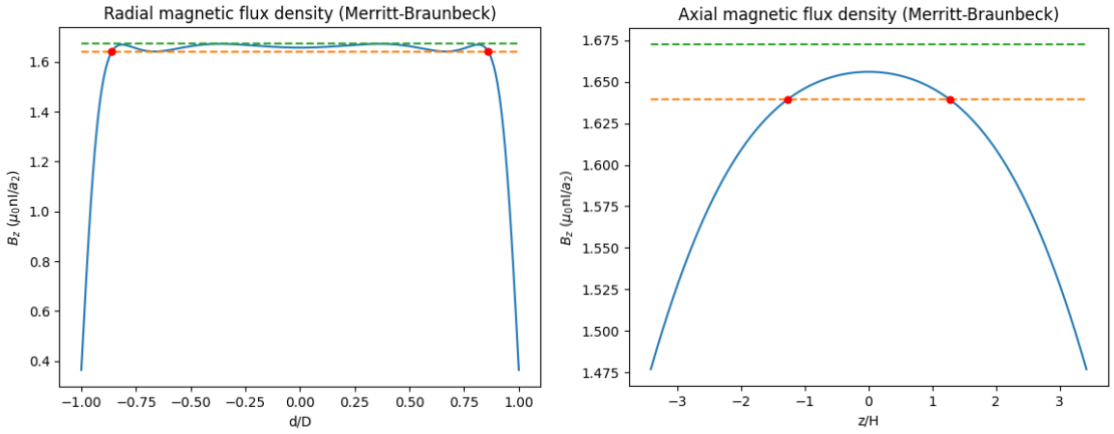

Figure 6. *Simulated* ***(a)*** *radial and* ***(b)*** *axial magnetic flux densities of the Merritt-Braunbeck configuration.*

Moreover, according to the same simulations, the magnetic field generated by the Merritt-Braunbeck configuration possesses two-fold symmetry, providing an equal trend in the magnetic flux density along the radial plane for orthogonal directions. A surface plot and a contour plot illustrating the distribution and variation of magnetic flux densities along the radial plane are shown in Fig. 7a and Fig. 7b respectively.

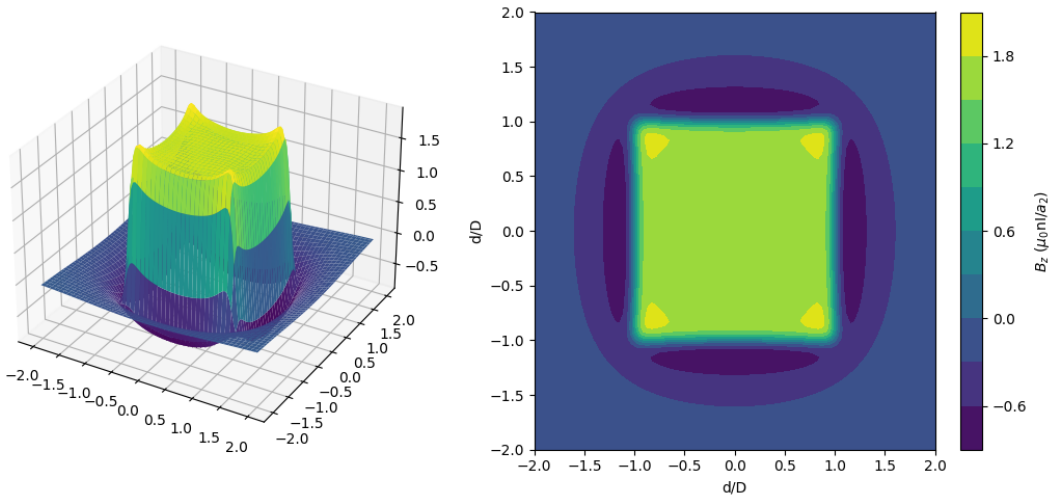

Figure 7. *Simulated* ***(a)*** *3D surface plot and* ***(b)*** *2D contour plot depicting magnetic flux densities along the radial plane.*

We now present our experimental findings. As mentioned previously, measurements of the magnetic flux density within the Merritt-Braunbeck setup were taken using the triple-axis gaussmeter along regular intervals of 5mm. The line plots depicting the magnetic flux densities across all three axes are shown in Figure 8a, 8b, and 8c, where we take the x-axis and y-axis to be the radial axes, and the z-axis to be the axial axis.

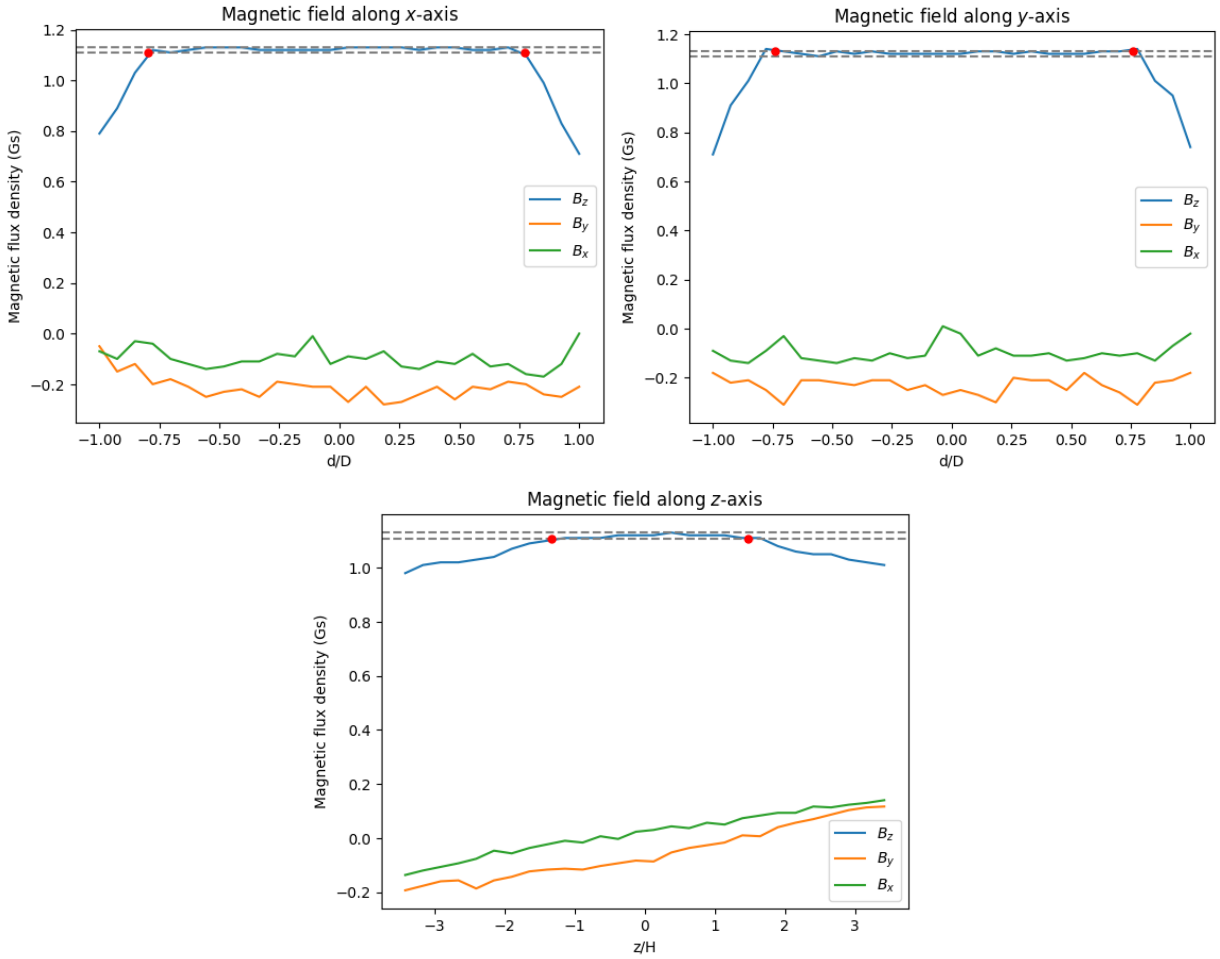

Figure 8. *The magnetic flux densities generated by the Merritt-Braunbeck coils across* ***(a)*** *the x-axis,* ***(b)*** *the y-axis, and* ***(c)*** *the z-axis.*

The field has a B_z value of approximately 1.12Gs at the origin, and spatially varies in a manner similar to the aforementioned simulations. The B_x and B_y values appear to fluctuate randomly throughout the radial plane, but generally follows an increasing trend as the sensor moves upwards along the axial plane. Similar to Fig. 6, the grey dotted lines represent the upper and lower bounds for the homogeneity threshold for the B_z value, and the red points represent the lines of intersection between the magnetic flux density and the homogeneity threshold. The acceptably homogenous lengths span 78.5%, 77.6%, and 150.3% of the x, y, and z axes respectively, giving a mean radial homogeneity of 78.05% when taking the average of the both the x and y axes.

5 Discussion & Conclusion

With reference to the mathematical parametric equation derived from the Biot-Savart law, the Merritt-Braunbeck coil configuration offers a 231.4%, 128.5%, and a 231.8% increase in magnetic flux density experienced at the origin when compared to the Helmholtz, Braunbeck, and Merritt four-coil configurations respectively, given a constant number of coils, current amperage, and radius length. This shows that the Merritt-Braunbeck coil configuration performs excellently in generating a strong magnetic field, more than doubling the magnetic flux density created by the Helmholtz and Merritt coil configurations.

Experimental testing of the Merritt-Braunbeck coil configuration aligns closely to the computational simulations visualised using Magpylib in Python. The homogeneity metric of the field generated by the Merritt-Braunbeck has an average radial d/D value of 78.05% and an axial z/H value of 140.5%. The radial homogeneity is significantly superior compared to other existing coil geometries, boasting a 203.6%, 127.3%, and an 119.7% increase in the d/D metric with regards to the Helmholtz, Braunbeck, and Merritt configurations respectively for helical coiling methods. However, this admittedly comes at the expense of the z/H metric, which underperformed in comparison to the Braunbeck and Merritt coil configurations, possessing a subpar 65.8% and 50.2% of their respective axial homogeneities. Furthermore, there appears to be erratic variations in the B_x and B_y values across all axes, which may be caused by imperfect coiling of the frames, leading to stray magnetic fields interfering with the results.

Overall, the Merritt-Braunbeck magnetic coil configuration holds significant promise for a spectrum of quantum-related applications. The enhanced uniformity and strength of the generated fields are pivotal for manipulating states and facilitating precise control over quantum systems. The Merritt-Braunbeck magnetic coil configuration can be used in the realm of quantum sensors, communication, and computing, which relies on uniform magnetic fields for highly-sensitive measurements of quantum states, enabling the development of superior technologies. The improved optical access also increases the feasibility of integrating quantum setups into both compact and versatile systems. With regards to the methodology, the choice of additive manufacturing using PLA+ filament was motivated due to its cost-effectiveness and convenience. However, 3D-printed plastics are certainly limited by their mechanical durability, which could be detrimental to the overall sturdiness of the setup. Additionally, the coiling of the wires was imperfect due to challenges faced when inserting the wires into clips and power supplies, which contributed to heightened levels of unwanted noise as depicted within our experimental results. Other coiling methods, such as pancake coiling, were also largely unexplored via experimental methods, as we only constructed a coil configuration with helical coiling in this paper, thus raising the possibility of more suitable configurations being overlooked. To address these limitations, future investigations could explore alternative materials with better mechanical properties, refine the coiling process through automated or industrial means to achieve a neater structure, and conduct extensive research on the effects of different coiling methods with regards to field homogeneity and strength. These changes may potentially elevate the performance of the magnetic configuration and eliminate background noise.

References

[1] Lett, P. D., Phillips, W. D., Rolston, S. L., Tanner, C. E., Watts, R. N., & Westbrook, C. I. (1989). Optical molasses. *Journal of the Optical Society of America B-optical Physics*, *6*(11), 2084. https://doi.org/10.1364/josab.6.002084

[2] Vilas, N. B., Hallas, C., Anderegg, L., Robichaud, P., Winnicki, A., Mitra, D., & Doyle, J. M. (2021). Magneto-Optical trapping and Sub-Doppler cooling of a polyatomic molecule. *arXiv (Cornell University)*. https://doi.org/10.1038/s41586-022-04620-5

[3] Wu, B., Zhu, D., Cheng, B., Wei, L., Wang, K., Wang, Z., Qing, S., Li, R., Wang, H., Wang, X., & Lin, Q. (2019). Dependence of the sensitivity on the orientation for a free-fall atom gravimeter. *Optics Express*, *27*(8), 11252. https://doi.org/10.1364/oe.27.011252

[4] Lin, S. T., & Kaufmann, A. (1953). Helmholtz coils for production of powerful and uniform fields and gradients. *Reviews of Modern Physics*, *25*(1), 182–190. https://doi.org/10.1103/revmodphys.25.182

[5] Braunbeck, W. (1934). The Generation of Largely Homogeneous Magnetic Fields by Circular Currents. *Zeitschrift Für Physik*, *88*(5–6), 399–402.

[6] Merritt, R. P., Purcell, C., & Stroink, G. (1983). Uniform magnetic field produced by three, four, and five square coils. *Review of Scientific Instruments*, *54*(7), 879–882. https://doi.org/10.1063/1.1137480

[7] Spengler, N., While, P. T., Meissner, M., Wallrabe, U., & Korvink, J. G. (2017). Magnetic Lenz lenses improve the limit-of-detection in nuclear magnetic resonance. *PLOS ONE*, *12*(8), e0182779. https://doi.org/10.1371/journal.pone.0182779

[8] Bono, J. T., & Purpura, J. W. (2017). Theory Behind Coil-Geometry Parameters for Fanselau/Braunbeck Magnet Coils. *Naval Surface Warfare Center, Panama City Division*, 18–22.

[9] Magdaleno-Adame, S., Olivares-Galvan, J. C., Campero-Littlewood, E., Escarela-Perez, R., & Blanco-Brisset, E. (2010). Coil systems to generate uniform magnetic field volumes. In *Excerpt from the proceedings of the COMSOL conference* (Vol. 13, pp. 401-411). Massachusetts, USA: COSMOL, Inc, Lindsay Paterson.

[10] Ortner, M., & Bandeira, L. G. C. (2020). Magpylib: A free Python package for magnetic field computation. *SoftwareX*, *11*, 100466. https://doi.org/10.1016/j.softx.2020.100466

[11] Virtanen, P., Gommers, R., Oliphant, T. E., Haberland, M., Reddy, T., Cournapeau, D., Burovski, E., Peterson, P., Weckesser, W., Bright, J., Van Der Walt, S. J., Brett, M., Wilson, J., Millman, K. J., Mayorov, N., Nelson, A., Jones, E. D., Kern, R., Larson, E. B., . . . Vázquez-Baeza, Y. (2020). SciPy 1.0: fundamental algorithms for scientific

computing in Python. *Nature Methods*, *17*(3), 261–272. https://doi.org/10.1038/s41592-019-0686-2

[12] Nelder, J. A., & Mead, R. (1965). A simplex method for function minimization. *The Computer Journal*, *7*(4), 308–313. https://doi.org/10.1093/comjnl/7.4.308

Annex

This annex serves to provide additional graphics and figures illustrating the simulations of the homogeneity metrics provided in Table 1.

For the filamentary Helmholtz coil configuration,

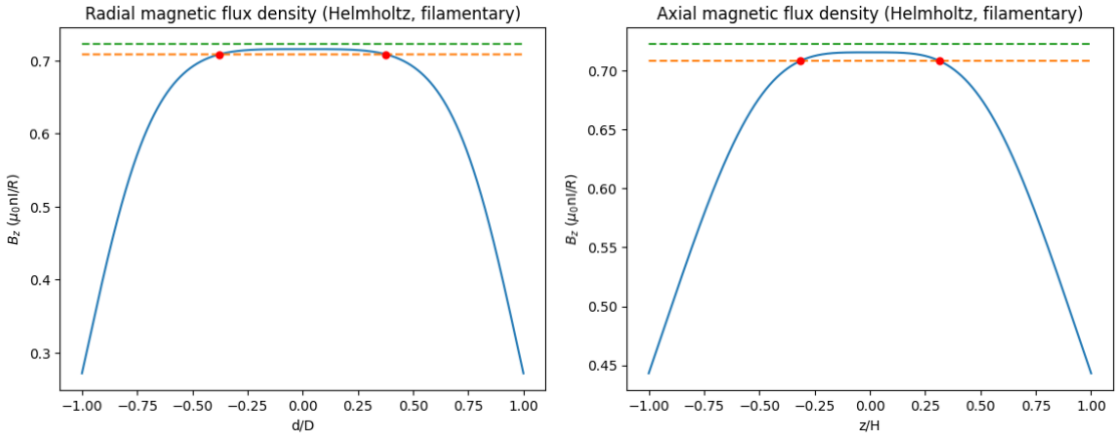

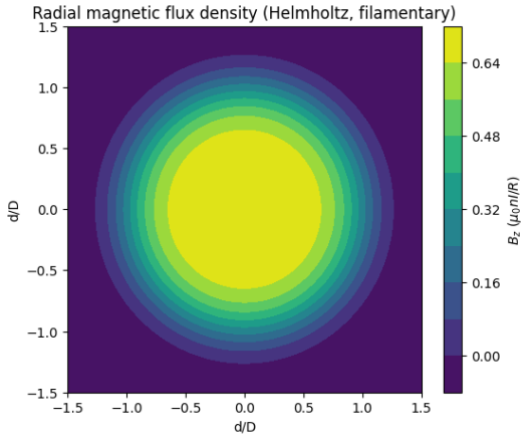

For the helical Helmholtz coil configuration,

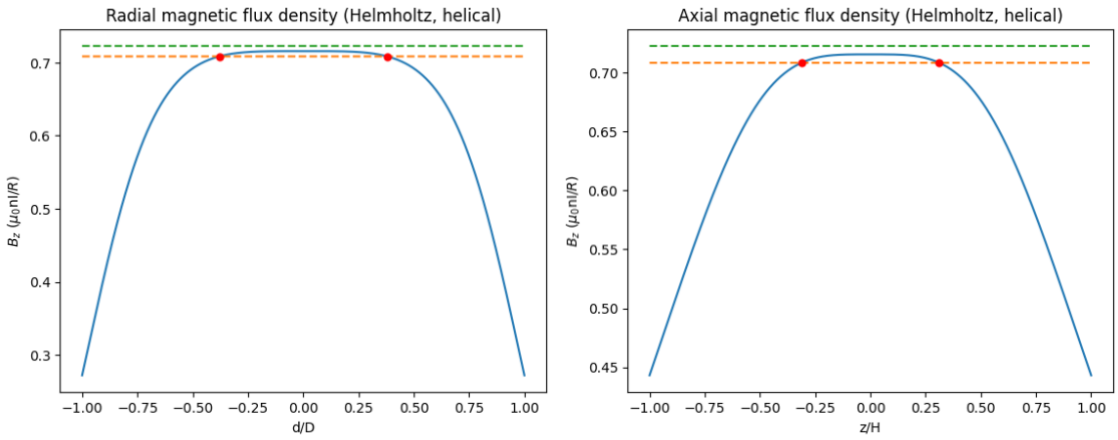

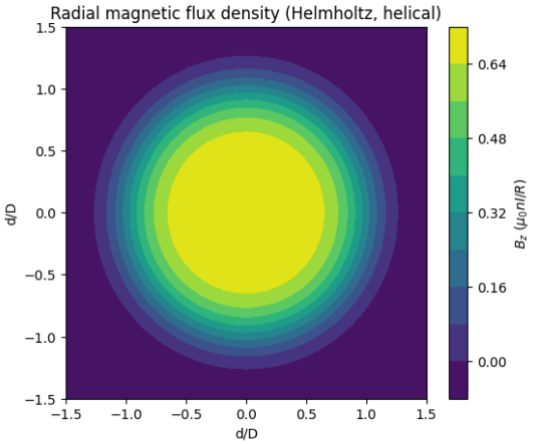

For the pancake Helmholtz coil configuration,

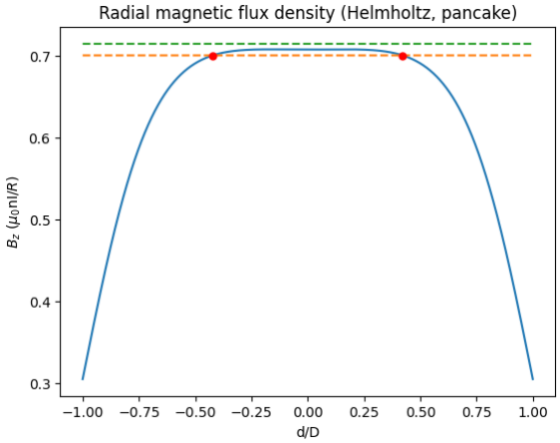

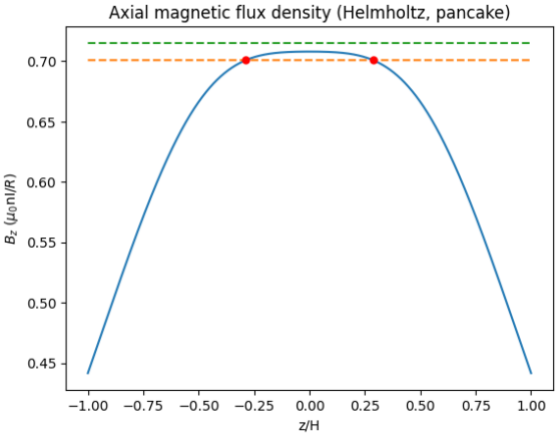

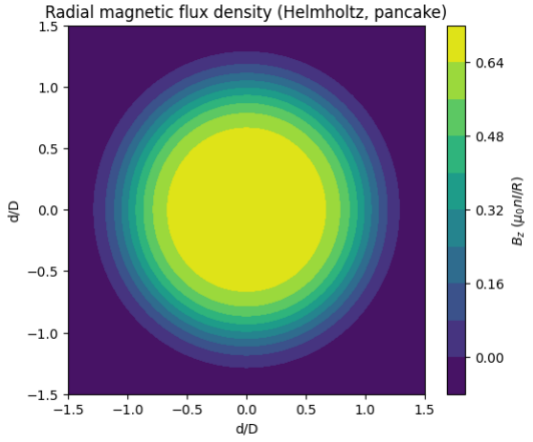

For the filamentary Braunbeck coil configuration,

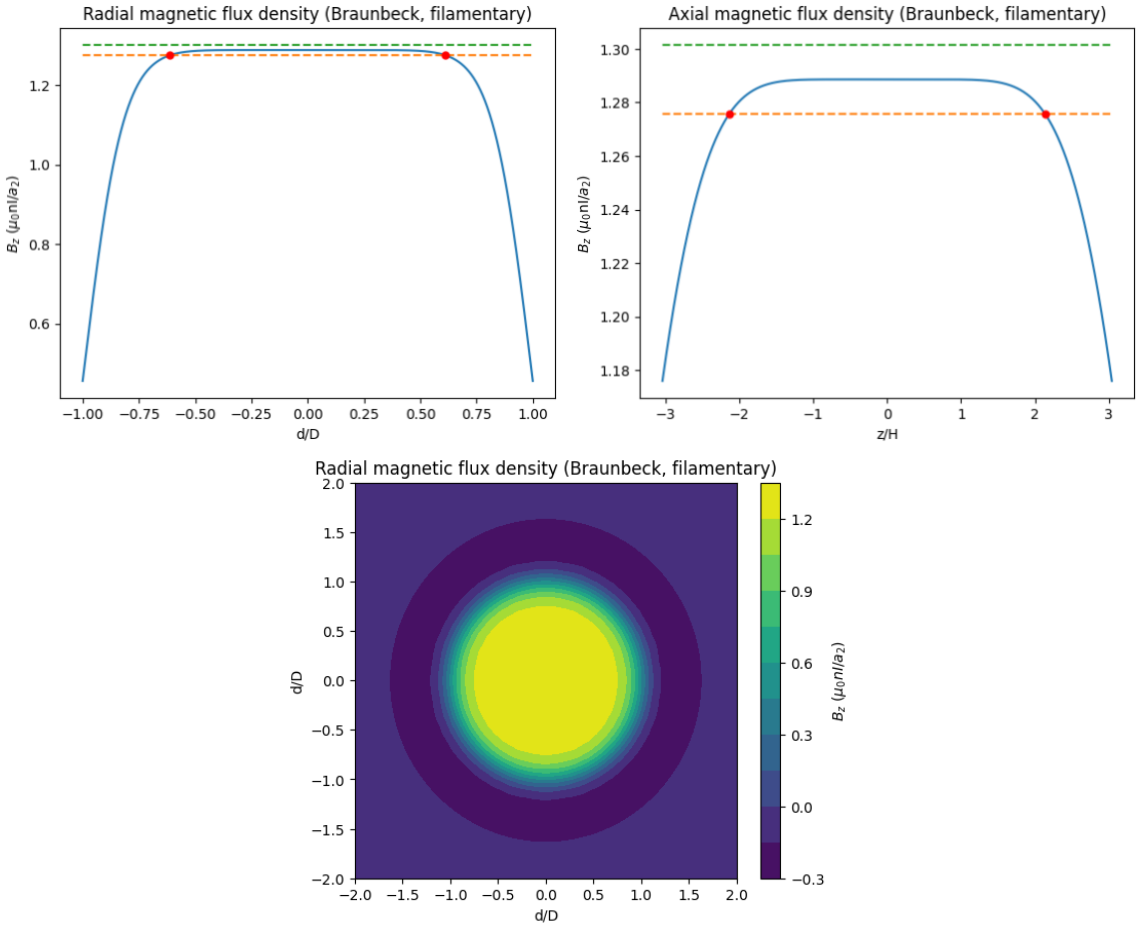

For the helical Braunbeck coil configuration,

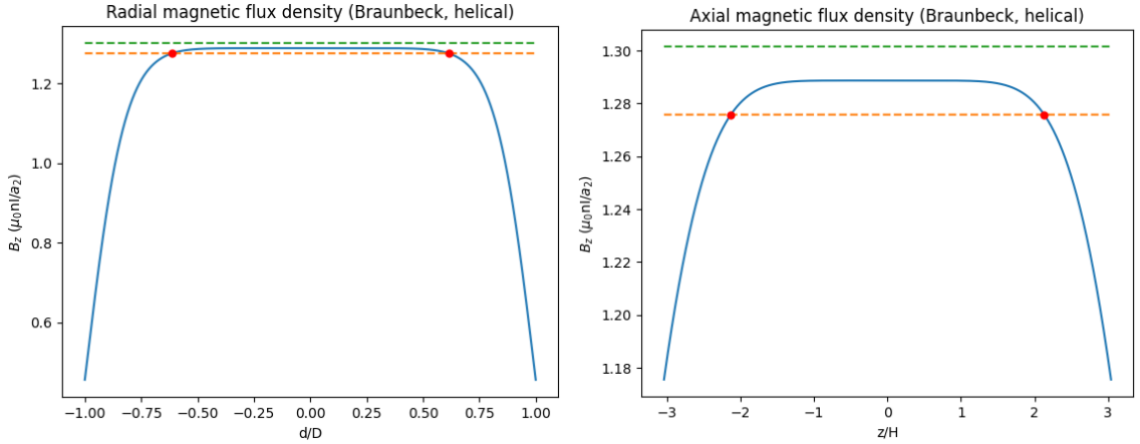

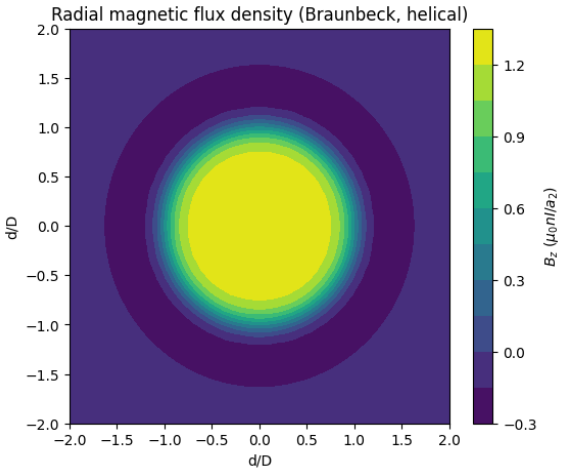

For the pancake Braunbeck coil configuration,

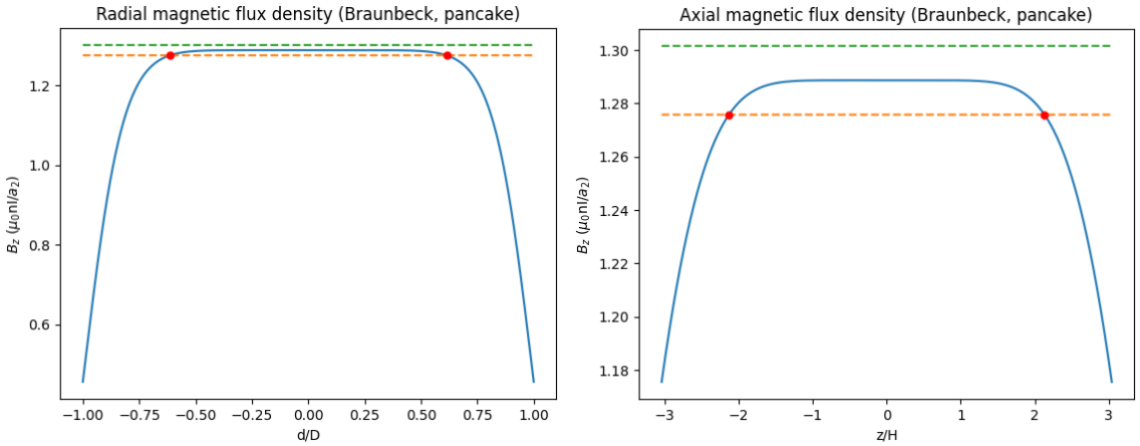

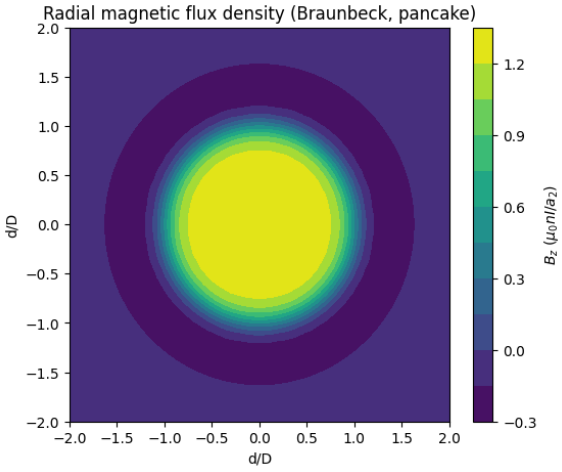

For the filamentary Merritt four-coil configuration,

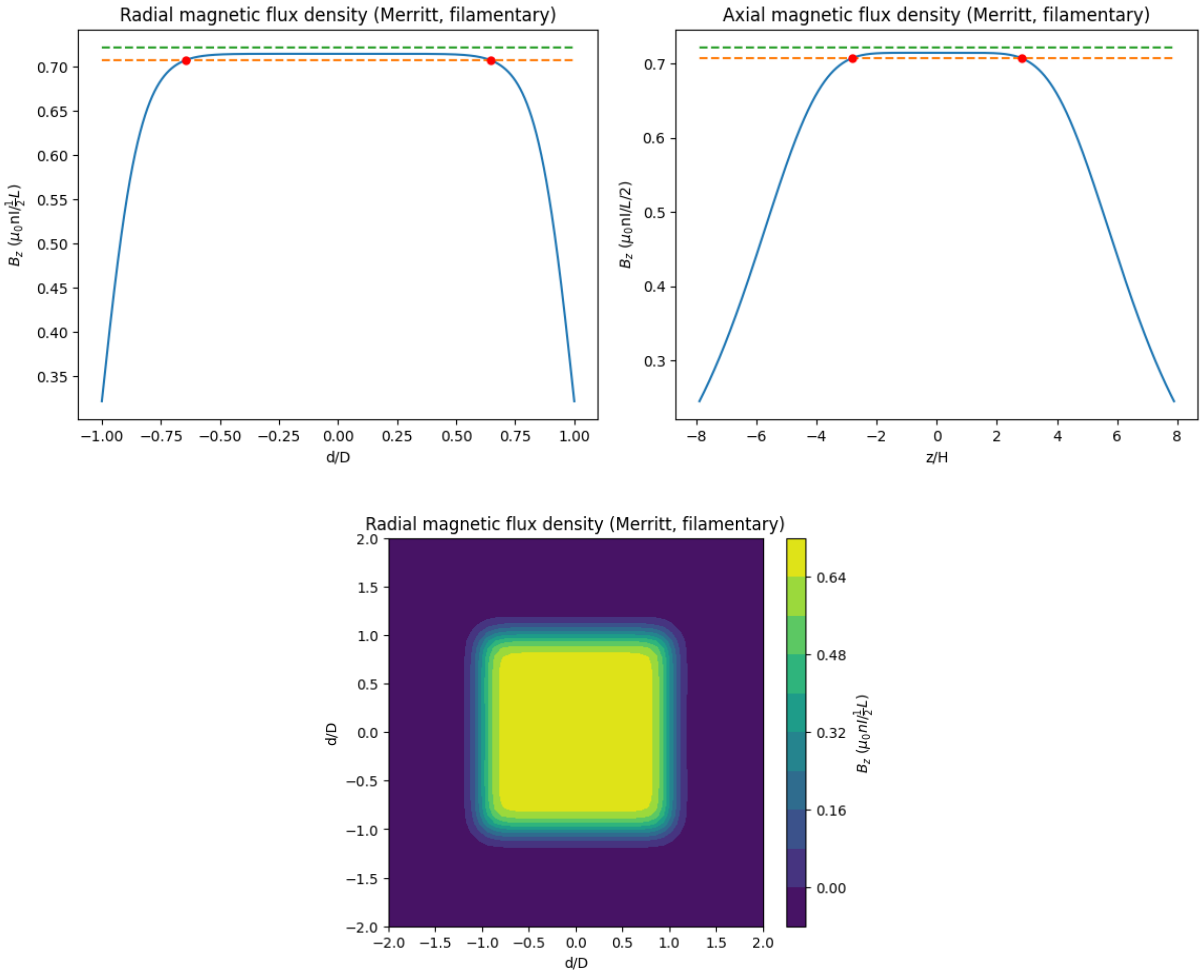

For the helical Merritt four-coil configuration,

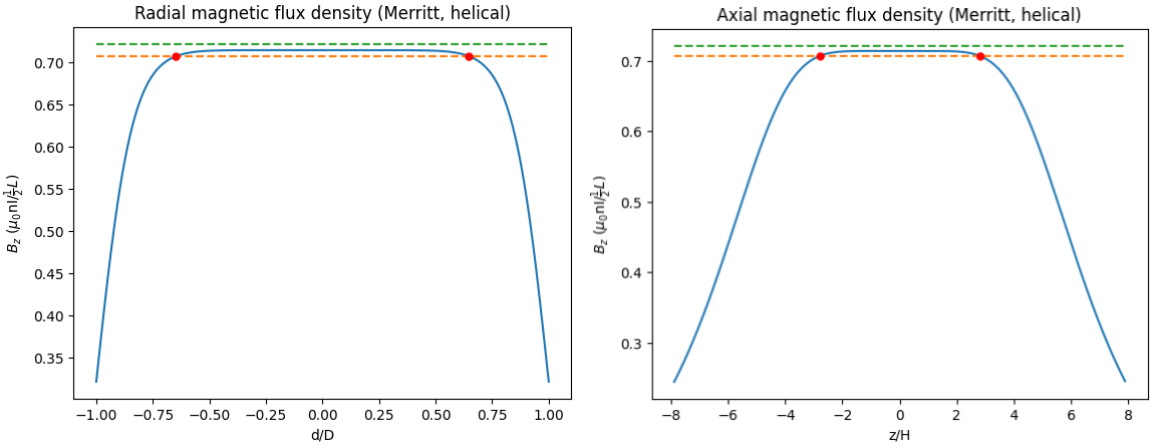

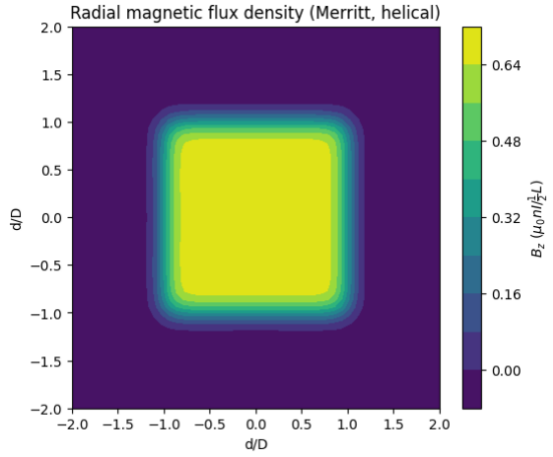

For the pancake Merritt four-coil configuration,